

Scatterometer Wind Speed Bias Induced by the Large-Scale Component of the Wave Field

R. E. GLAZMAN, G. G. PIHOS,¹ AND J. IP²

Jet Propulsion Laboratory, California Institute of Technology, Pasadena

The entire set of Seasat A satellite scatterometer (SASS) wind speed observations, U_s , colocated with the buoy measurements of the wind speed U_b and wave height $H_{1/3}$ is analyzed. The "error" $U_b - U_s$ is found to be influenced by the degree of wind-wave coupling. This coupling is quantified employing the ratio of the wave-to-wind energy densities: $X \sim \rho_w g \langle \zeta^2 \rangle / \rho_a U_b^2$. For the special case of a fetch-limited wave growth, X is shown to coincide with the wind fetch. It is found that when the coupling is weak, i.e., at large X , the SASS tends to overestimate the wind speed, and vice versa. The magnitude of the trend is evaluated roughly as 0.5 m/s per 100 km of X . The increased radar backscatter at large X is explained by invoking the concept (due to V. Zakharov and his collaborators) of a Kolmogorov equilibrium range appearing in wave spectra of sufficiently developed seas when the wind input is concentrated at high frequencies. In this extreme case, the surface density of steep wavelet occurrence would be at its highest owing to a pronounced cascade pattern in the surface geometry. The fractal dimension D_H of such an idealized surface is estimated to be about 2.333. Further, it is suggested that D_H for a general case is a function of sea maturity. Finally, it is concluded that both the probability and the surface density of steep wavelet events are increasing functions of X . A major implication with respect to the electromagnetic scattering is that the so-called spike component of the backscattering coefficient, formed from the individual radar returns caused by the steep and/or breaking wavelets, is controlled primarily by the large-scale features of surface geometry, hence by such nonlocal factors of the wave development as the wind fetch.

1. INTRODUCTION

In recent years the interest in environmental factors that can bias satellite scatterometer measurements of wind speed increased significantly. Much attention has been paid to the possible impacts of atmospheric stability [Keller *et al.*, 1985; Liu, 1984], sea surface temperature (SST) [Liu, 1984; Woiceshyn *et al.*, 1986; Donelan and Pierson, 1987], and large-scale wave slope [Plant *et al.*, 1983] on the radar return in the X and K_u bands of electromagnetic (em) waves (the scatterometer frequencies). The goal of the present work is to determine if an environmental bias exists in the winds measured by the Seasat A satellite scatterometer (SASS) as caused by variations in the degree of wind-wave coupling. As a possible measure of this coupling, one can employ the wind fetch. If the fetch-related bias does exist, the global wind maps based on scatterometer measurements would contain false climatic trends. For instance, the winds in the regions of trade winds and westerlies where the wind-wave coupling is relatively weak (the fetch is large) would be systematically exaggerated, as we show in this paper, whereas the winds in the areas and seasons characterized by fast-moving deep lows (the fetch is small and the wind-wave coupling is strong) would be biased in the opposite direction.

Our research effort includes the analysis of colocated observations done by the SASS (using the SASS I model function) and by the buoys of the National Data Buoy Center (NDBC) (section 3) as well as the theoretical considerations concerned with wind-wave dynamics and sea surface statistical geometry (sections 2 and 4). The latter part of the work is rather qualita-

tive: it is based on critical analysis of several recent publications on wind waves and statistical geometry and is intended to help interpret the experimental results and formulate a hypothetical model (section 5) for physical mechanisms responsible for the trend.

In sections 3.3 and 3.4 we show that a bias in the SASS winds due to variations in the degree of wind-wave coupling is well pronounced. Our result seems to contradict the conclusion made by Ross and Jones [1978] that the degree of wave development (i.e., the wind fetch) is unimportant. However, as we show in section 3.4, variations of the fetch yielding appreciable effects on the backscatter span a range much broader than that covered by the Ross and Jones experiment. The SASS-wind error trend is estimated roughly to be about 0.5 m/s per 100 km of the generalized wind fetch. In order to explain the observed trend, we present arguments (section 4) indicating that certain basic properties of the sea surface, such as its effective (fractal) dimension characterizing a cascade pattern in surface geometry, are greatly influenced by the degree of wind-wave development.

The determination of environmental trends is connected with certain difficulties. Indeed, if a trend is responsible for only a small fraction of the total rms error (nonetheless remaining important for all those cases where an environmental variable causing the bias differs significantly from its mean value), the common techniques such as regression analysis will not reveal it convincingly: the trend is masked by random errors due to instrument and data processing contributions to the total measurement noise and by various intervening factors such as inhomogeneity of the wind field within a single SASS footprint. To make things worse, we have to deal with an ill-defined quantity, the SASS error, that is obtained by subtracting the SASS wind averaged over the surface footprint representing some 1400 km² from the buoy wind obtained by time averaging of wind speed recorded at a fixed point. An approach to resolving the difficulty is proposed in section 3.2 based on forming "super observations" from a relatively few

¹ Now at Aerospace Corporation, Los Angeles, California.

² Now at Dartmouth College, Hanover, New Hampshire.

Copyright 1988 by the American Geophysical Union.

Paper number 7C0823.
0148-0227/88/007C-0823\$05.00

cases of large errors while assigning a relatively low weight to the cases where the errors are small.

2. EFFECTS OF LARGE-SCALE WAVES ON SCATTEROMETER RESPONSE

Here, the basic physical concepts concerned with effects of large-scale waves on microwave radar return are considered. This section will provide the background for our experimental approach and will facilitate the interpretation of the results. In what follows, the large-scale wave component is defined as the wind-generated gravity waves which constitute the first, and possibly second, decade of the wave spectrum: from the spectral peak through the equilibrium range. The small-scale roughness in the present consideration is associated with capillary and capillary-gravity waves.

2.1. The Backscattering Cross Section

The geophysical model functions presently available relate the radar cross section directly to an instantaneous local wind vector: $\sigma^0 = f(U)$. Such relationships presume that the backscatter is due mainly to the Bragg-resonant small-scale ripples which are produced by the local wind stress on a given surface patch. Another assumption implicit here is that the long-range (i.e., nonlocal) factors which might manifest themselves through an impact of the large-scale wave component on the X band scattering (e.g., by tilting and straining of the rough surface facets) are of little importance. Indeed, the gravity waves have a much greater relaxation time than the small-scale ripples, and they are not necessarily caused by the instantaneous local wind. This is so because the characteristic time for energy exchange among the resonant wave modes is of the order of $\tau/(\nabla\zeta)^2$ [Phillips, 1960], where τ is the corresponding wave period, which amounts to several hours necessary for the equilibrium range of the wave spectrum to adjust to a change in wind speed. Hence accounting for the nonlocal mechanisms of the wind wave development would require the inclusion of long-range factors (for instance, the wind fetch or the rate of wind speed increase/decrease over the last few hours) into the geophysical model function.

Let us assume first that the large-scale waves affect the X band scattering indirectly in the fashion described by the two-scale model [Wright, 1968]. Then, the relative importance of wind fetch can be inferred from the analysis of its effect on the rms tilt of the rough facets. For a fetch-limited sea one may employ the mean Joint North Sea Wave Project (JONSWAP) spectrum, which yields

$$\langle |\nabla\zeta|^2 \rangle \approx g^{-2} \langle (\partial^2\zeta/\partial t^2)^2 \rangle = g^{-2} M_4 \approx 0.055(U_{10}^2/gX)^{0.2} \quad (1a)$$

Here, the linear-wave dispersion relation was used, and the fourth-order spectral moment

$$M_4 = \int_0^\infty S(\omega)\omega^4 d\omega \quad (1b)$$

was evaluated by Glazman [1986]. The calculation of M_4 involved partial averaging of the surface, with the averaging scale well exceeding the characteristic wavelength of Bragg-resonant ripples. Using (1a), one finds that the large-scale slope is small regardless of the degree of wave development. For such a case, the two-scale model yields for moderate incidence angles a linear dependence of the radar cross section on

the wave slope variance, for both horizontal and cross polarizations, and the case of vertical polarization turns out to be independent of the tilt [Wright, 1968]. Furthermore, direct computations using (1a) show that relative deviations of the rms slope due to possible variations of the fetch are negligibly small. Hence, even for the cases of σ_{hh}^0 and σ_{vh}^0 , the two-scale model would not be capable of explaining appreciable influence of the long-range factors, such as wind fetch, on the X band scattering.

However, in addition to the indirect influence of the large-scale tilt, there is a direct impact of the gravity range waves on the scatterometer response. Numerous investigations show that a non-Bragg mechanism of surface scattering emerges at sea in the presence of gravity range wavelets with sharp and/or breaking crests [Kalmykov and Pustovoytenko, 1976; Skolnik, 1980; Lyzenga et al., 1983; Kwoh and Lake, 1984, 1985]. Its manifestations have been directly observed only as intermittently occurring spikes in the radar return, provided the illuminated area was sufficiently small to include just one or few of the spike-generating wavelets. Although some laboratory investigations [e.g., Kwoh and Lake, 1984] have shown these wavelets to have a steep slope and/or breaking crest, the actual mechanism of the em wave scattering from these wavelets as well as their local geometry are not well known. An important difference between the observations of sea spikes and the satellite scatterometer measurements is due to the size of the illuminated area. The mean SASS footprint is about 1400 km². Anticipating a large number of steep wavelets to be present within this area, one can average all quantities over the surface. Let us write the mean surface density of the spike-caused component of σ^0 in the form

$$\sigma_s^0(\Theta) = \int_0^\pi \int_\Gamma^\infty n(\gamma, \theta - \Theta) \sigma^1(\gamma, \theta) d\gamma d\theta \quad (2)$$

Here $n(\)$ is the mean surface density of wavelets with steepness γ oriented at azimuthal angle $\theta - \Theta$ with respect to the radar beam; σ^1 is the mean backscattering coefficient for an individual wavelet. Γ is the minimal steepness necessary to generate a spike in the radar return at a given radar geometry (this Γ is probably close to the critical steepness of a wave before breaking [Skolnik, 1980, chapter 13.3]). The incidence angle dependence is implied. The local geometry of the "ringing" wavelet determines the value of σ^1 , whereas the statistics of such wavelets' occurrence are contained in $n(\)$.

In section 5 it is suggested that the relative variations of σ^1 caused by possible variations in wind wave conditions are likely to be small compared to the variations of $n(\)$. If this is true, we can focus the attention on the rate of occurrence of steep and/or breaking wavelets. Since $n(\)$ pertains to the large-scale waves (as defined earlier), we anticipate it to be controlled not only by the local instantaneous wind but also by other factors of wind wave development. For the case of the mean JONSWAP spectrum, the importance of wind fetch in statistics of large-scale wavelets has been demonstrated earlier [Glazman, 1986]. In particular, the surface density for the events of steep wavelet occurrence has been shown to be

$$\nu(\Gamma) = \frac{\sqrt{3}}{(2\pi)^{3/2}8g} \frac{M_8}{M_4} \frac{\Gamma}{\sqrt{M_4}} \exp \left[-\frac{(g\Gamma)^2}{2M_4} \right] \quad (3)$$

where $\nu(\Gamma)$ is defined as the mean number of wavelets whose steepness $|\nabla\zeta|$ is greater than Γ that occur simultaneously per

unit area of sea surface. M_i is an i th-order spectral moment. This relationship was discussed in detail by Glazman [1986], and the factor

$$P(\Gamma) = \frac{(2\pi)^{1/2}\Gamma}{M_4^{1/2}} \exp\left[-\frac{(g\Gamma)^2}{2M_4}\right] \quad (4)$$

entering (3) was interpreted as the probability for an individual wavelet to have the slope $|\nabla\zeta|$ exceeding Γ .

The behavior of ν for a special case of the limiting slope Γ equal to 0.3, which is close to a "breaking wave criterion," is depicted in Figure 6 of Glazman [1986]. However, the mean JONSWAP model used in that calculation is hardly applicable if the fetch exceeds some 70 km (see sections 4.1 through 4.3 for further discussion). Nevertheless, the plot is interesting in that it demonstrates how the fetch variations can cause order of magnitude changes in ν .

Furthermore, the $n(\gamma, \theta)$ of (2) is related to the ν by

$$\nu(\Gamma) = \int_0^\pi \int_\Gamma^\infty n(\gamma, \theta) d\gamma d\theta \quad (5)$$

The inside integral can be replaced with some $N_{\Gamma}(\theta)$ understood as

$$N_{\Gamma}(\theta) = \int_\Gamma^\infty n(\gamma, \theta) d\gamma \sim (\Gamma_{cr} - \Gamma)n(\Gamma, \theta) \quad (6)$$

This implies that due to the breaking of steep wavelets, the mean number of wavelets with $\gamma > \Gamma$ drops off rapidly and vanishes when the critical steepness Γ_{cr} is attained. Then, one can use (3) to predict the behavior of $n(\gamma, \theta)$ in (2).

Equations (1) and (3) are employed here to illustrate that in contrast to the wave slope variance, the surface density of steep wavelet events is a strong function of sea maturity. Hence it is the spike-producing events of steep wavelets, rather than the tilting of the rough patches by large-scale waves, that might yield manifestations of the degree of wind-wave coupling in the SASS radar return. We shall adopt this qualitative view as a hypothesis to be referred to in the course of our data analysis.

2.2. Quantitative Measures of Large-Scale Wave Effects

We need an appropriate parameter to characterize the non-local effects of wind on the wave field. A natural choice would be wind fetch and/or duration. However, these measures of wind-wave coupling are difficult to evaluate. For instance, the fetch can be unambiguously determined only in the special case of a stationary and spatially uniform wind field with the wind vector directed along the outward normal to the straight coastline. Besides, all we have at our disposal is scanty information on the environmental conditions as reported once every hour, and in many cases once every 3 hours, by sparsely spaced buoys of the National Data Buoy Center. In view of these difficulties, we introduce a new measure of the long-range wind influence which can be employed when only the local wind speed and significant wave height are known. We define it as the ratio of the mean potential energy density (per unit surface area) of wind waves to the kinetic energy density (per unit volume) of mean wind:

$$X = \text{const} \frac{\rho_w g \langle \zeta'^2 \rangle}{\rho_a U^2} \quad (7)$$

It is easy to see that the notions of "wave maturity" or "wave age" express the same idea as this X . Moreover, in special cases where the conventional wind fetch makes sense, the ratio (7) must be a monotonically increasing function of the fetch: at a given wind speed, the energy accumulated in the wave field must increase with the distance along the wind vector.

The total variance of the surface vertical displacement is related to the significant wave height reported by the buoys by $4 \langle \zeta'^2 \rangle^{1/2} \approx H_{1/3}$. Furthermore, in the appendix we suggest a rationale for a specific choice of the proportionality coefficient in (7). Ultimately, measure X can be calculated from

$$X = 3.4 \times 10^5 \frac{g H_{1/3}^2}{U_b^2} \quad (8)$$

where U_b is the wind supplied by a buoy, referenced to the 10-m height. In other words, $\text{const} \approx 26.1$. As is discussed in the appendix, this choice allows one to tentatively refer to X as the wind fetch. However, the X introduced here has a much broader meaning than the conventional fetch, and it would be incorrect to extend the interpretation of X as the conventional fetch, as offered in the appendix, to the situations where the JONSWAP model and, more importantly, the Phillips law do not apply. Such situations will be discussed in greater detail in section 4.

3. ANALYSIS OF SASS WIND SPEED MEASUREMENT ERRORS

3.1. SASS and NDBC Data

The SASS-NDBC colocated data set was compiled from several sources. We obtained sets of unambiguous scatterometer wind speed and direction data from NASA Goddard Space Flight Center (GSFC) in Greenbelt, Maryland (thanks are due to R. Atlas), for the entire Seasat mission and from P. Woiceshyn of the Jet Propulsion Laboratory (JPL), Pasadena, California, for the period September 6–20, 1978. GSFC obtained from Atmospheric Environmental Service (AES) in Downsview, Ontario, Canada, a complete set of ambiguous scatterometer wind vectors processed onto a 100-km-resolution grid oriented along the satellite subtrack which was then used as input into their objective ambiguity removal scheme. Woiceshyn's group, working with the same AES data set, resolved the ambiguous wind directions manually from the 15-day subset of data. Both the GSFC and the JPL data sets contain vectors not processed by the other, and occasionally disagree with each other regarding the wind direction chosen although the differences in wind speeds are quite small. These two sources were melded into one data set containing approximately 2 million wind vectors. The NDBC data set, procured directly from the National Data Buoy Center, consists of approximately 25,000 observations from 19 moored buoys off the coasts of North America.

The unambiguous (dealias) wind vector data were then sorted against NDBC wind observations to match coordinates and observation times using a window of 100 km and 60 min. This yielded 2637 colocated observations. Although the colocated data set contains only 8.5% of the total buoy observations, the statistics for the colocated buoy observations are in very good agreement with those of the entire NDBC data set. Since the reported scatterometer wind speeds are the neutral stability wind speeds at 19.5 m and the in situ winds are measured by different buoys at different heights, the in situ

19.5-m neutral stability wind speeds were also calculated for each buoy observation using the technique of *Liu et al.* [1979].

3.2. Approach to Data Analysis

The variable under consideration,

$$\delta U = U_b - U_s \quad (9)$$

where U_s is SASS wind speed, is not well defined from the physical standpoint and contains much noise due to instrument and data processing errors from both SASS and NDBC. Some errors arise that are due to occasional large spatial/temporal distances between the SASS and NDBC observation locations/times, as well as due to various intervening factors (e.g., atmospheric vapor). As a result, the trend analysis contemplated here cannot be carried out as a usual correlation analysis: we are not seeking a dependence (linear or otherwise) of δU on X . We are looking for a bias that may manifest itself in a large volume of data, possibly along with other climatic trends that are not directly addressed in the present work. The major difficulty of the problem stems from the fact that the level of noise exceeds the signal level, thus greatly reducing the absolute value of correlation coefficients in possible regression models.

The following procedure has been introduced to increase the relative statistical weight of the "interesting" cases through the use of "super observations". Let a_i be a set of N criteria discriminating more interesting cases from less interesting ones. Consider the centered SASS-NDBC difference,

$$e = \delta U - \delta \bar{U} \quad (10)$$

where $\delta \bar{U}$ is obtained by averaging over the entire data set. The cases rendered as most interesting are, for example, those for which $e > m\sigma_e$ and $e < -m\sigma_e$, where σ_e is the centered rms SASS-NDBC difference and m is about 2. Hence the a_i may characterize the intervals of $\delta U - \delta \bar{U}$ variation referenced to its rms value. It is desirable to choose a_1 and a_N such that the signal-to-noise ratio for all the cases in these extreme categories is as large as possible (say, not smaller than 2). Next, consider the cases for which the signal-to-noise ratio is lower by a specified amount, for instance: $(m-1)\sigma_e < |e| < m\sigma_e$, etc. Finally, we form one or several categories in which the signal-to-noise ratio is low. These latter cases are the least interesting. However, most of the observations will fall into just such high-noise groups. The number of observations falling into each category must be sufficiently large to provide statistically significant results. Hence the choice of criteria a_i is important.

Having tried several different choices, we have picked the most natural and simple set of criteria: $a_i = \pm(N-i)\sigma_e$ where $i = 1, 2, \dots, N$. For $N = 3$, this choice generates six groups of data, as listed in Table 1, with the volume of each group appearing sufficient to treat these groups as super observations. We expect the most interesting information to be found in groups 1, 2, 5, and 6, whereas groups 3 and 4 (containing over 70% of all data) will be the least informative.

To characterize the super observations thus obtained, two more tables have been produced. Table 2 gives the breakdown of the SASS (centered) errors, e , by the NDBC stations collocated with them. This breakdown suggests a possible trend in the geographic distribution of the SASS wind speed error (see Figure 1). For instance, the SASS measurements collocated with the Pacific NDBC stations appear, on the average, to

TABLE 1. Designation of Data Groups

Group	Interval of e	Number of Cases
1	$-\infty$ to $-2\sigma_e$	28
2	$-2\sigma_e$ to $-\sigma_e$	112
3	$-\sigma_e$ to 0	383
4	0 to σ_e	453
5	σ_e to $2\sigma_e$	110
6	$2\sigma_e$ to ∞	22

underestimate the wind speed. Table 3 gives the distribution of the SASS error by wind speed gradations, which show that at large wind speeds (over 10 m/s) SASS measurements tend to underestimate the wind, and at low winds (under 7.5 m/s) there is a hint of the opposite tendency. This tendency is well known (see, for example, *Freilich* [1986]). It has also been noticed by *Freilich* that SASS tends to overestimate the wind when the significant wave height reported by the NDBC observations is below its average value, and vice versa. Thus the question arises as to the existence of a basic physical mechanism causing all these trends.

3.3. Data Reduction and the Results of Data Processing

The data processing effort was carried out in two phases. First we used all the data available in the SASS-NDBC collocated data set and determined the mean error $\delta \bar{U}$ and the standard deviation σ_e of the centered error e : $\delta \bar{U} = 56$ cm/s; $\sigma_e = 199.6$ cm/s. These results are in good agreement with the Joint Air-Sea Interactions Project (JASIN) comparisons [*Jones et al.*, 1982] and with other estimates of the SASS wind speed accuracy [e.g., *Brown*, 1986]. With the σ_e so obtained we were able to group the data as shown in Table 1. However, owing to the collocation procedure, the input data set contained a large number of redundant and near-redundant cases: one buoy might be collocated with more than one SASS cell or with more than one vector dealiased by different techniques. Also, one SASS measurement might be collocated with two buoy observations (prior to and after an overflight). The redundancy has been reduced: wind speeds for the vectors that differed only in the dealiasing procedure employed were taken as the averages over all the aliases. The near-redundant cases such as the multiple buoy or SASS cell collocations have been reduced by selecting the "nearest neighbor."

In the second phase of the analysis we calculated the generalized wind fetch for each case of the collocated data, using (8). Both the mean fetch over all cases within a group and the standard deviation from the mean value have been determined for each of the six groups. However, due to the fact that some NDBC stations report the significant wave height with 3-hour intervals, the wave height was occasionally unavailable at the SASS overflight time (since the time window for collocation is 1 hour). Hence we had to obtain the buoy data for a greater time interval (up to 3 hours). Linear interpolation of the (relatively slow changing) wave heights allowed us to make use of some of such cases in the subsequent analysis. Eventually, a 15-hour interval was selected that included about 12 hours before and 3 hours after the SASS observation. This was used later to trace the process of wind field development or storm passage and, in some cases, to identify outliers. The set of

TABLE 2. Distribution of Observations by Error Gradations and by NDBC Stations

Buoy	Number of Colocated Observations						Total
	Group 1	Group 2	Group 3	Group 4	Group 5	Group 6	
41001	9	5	30	36	9	4	93
41002	0	0	0	1	0	0	1
42001	7	12	36	14	0	0	69
42002	0	5	14	8	1	0	28
42003	0	12	29	46	2	1	90
44001	0	2	3	0	0	0	5
44003	9	23	43	30	1	0	106
44004	0	7	28	26	5	1	67
46001	3	8	45	71	8	1	136
46002	0	13	63	62	19	0	157
46003	0	4	11	12	0	0	27
46004	0	3	9	22	8	2	44
46005	0	12	52	86	15	1	166
46006	0	6	20	39	42	12	119

these NDBC wind and wave histories played an important role in justifying the forthcoming data of Tables 3, 4, and 5.

Examination of the average wind fetch X for each group revealed a clear trend for the fetch to decrease with an increase of the group number. In other words, the scatterometer appeared to overestimate wind speed in the cases of large fetch and underestimate it in the case of small fetch. However, the large values of the fetch sometimes coincided with very low wind speeds. It is well known that the scatterometer accuracy drastically degrades at very low winds, and the causes of the greater errors at too low winds may be very different from the physical factors dealt with in the present work. Hence in order to decrease an impact of the cases that do not belong to the scope of the present research, we further reduced the input data set by eliminating all cases with NDBC wind speeds equal to or lower than 1.5 m/s. Along with the low wind speed cases, we excluded a few cases in which the wind fetch was either greater than 1250 km or smaller than 20 km. These values of X appeared unrealistic for the open ocean conditions, and they clearly stood out in the data set. The total relative number of such cases was less than 1%, while their influence was noticeable only in groups 1 and 6.

Finally, Table 4 was produced. It shows that the X -related bias is quite robust and manifests itself throughout the entire

range of X despite a great scatter in the values of X within individual groups. The resulting breakdown also allowed us to undertake a small cleaning of the data aimed at identifying cases having anomalous behavior with regard to this categorization. Many such cases were referred to as outliers and eventually rejected. To this end, we selected in each group the cases with conspicuously large departures of X from the mean values \bar{X} (greater than 2 standard deviations) and then examined the likely causes of such departures. Specifically, the history of the wind vector and significant wave height was studied to see if there was an anomalously fast change of wind speed and direction and/or significant wave height. Also, we checked for a particularly large spatial or temporal separations between the SASS and NDBC observations. As a result, most of the suspicious cases have been found to show anomalous deviations from the average conditions and, on these grounds, have been qualified as outliers. It turned out that most these outliers showed strong signs of the effects of swell on the significant wave height, such as a downward trend in wind speed and/or a sharp turn in the direction of wind in the preceding hours, accompanied by either constant or sometimes growing wave height. The total number of outliers, as shown in the resulting Table 5, is rather small (about 4.5%). However, the rms deviations given in the fifth and sixth columns changed appreciably. The elimination of the outliers has resulted in a pronounced increase in the strength of the X related bias.

Tables 4 and 5 summarize major results of this phase. The interpolation consistent with the idea of super observations requires specification of the significance level. We consider two levels: 80 and 95%. Assuming the Gaussian statistics for individual points within each group (which is acceptable for groups 2 through 5 and marginally acceptable for groups 1 and 6), the confidence intervals for the wind fetches have been obtained based on the Student distribution. The vertical bars are unnecessary, since the wind speed error in each group varies within a narrow range indicated in Table 1. In Figure 2 we present the X -related trend for two cases: 80 and 95% significance level as based on the results of Table 5. Evidently, even a level as high as 95% allows one to easily discern the X -related trend in the SASS error.

Although helpful for qualitative analysis of physical phenomena, the super observations based on the measurement

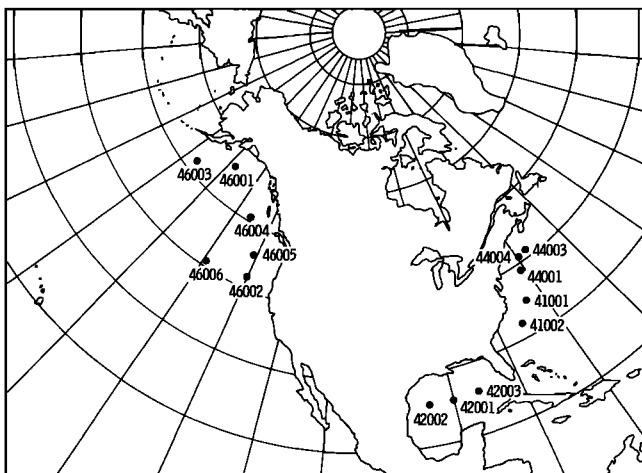


Fig. 1. NDBC stations employed in the data analysis.

TABLE 3. Distribution of Observations by Error and Wind Gradations

Wind Speed Gradation, m/s	Number of Colocated Observations						Total
	Group 1	Group 2	Group 3	Group 4	Group 5	Group 6	
0.0–2.5	8	9	31	21	0	0	69
2.5–5.0	6	19	63	112	21	0	221
5.0–7.5	10	42	124	136	28	0	340
7.5–10.0	3	30	111	92	26	4	266
10.0–15.0	1	12	50	79	34	13	189
15.0–20.0	0	0	4	11	1	4	20
20.0–∞	0	0	0	2	0	1	3

error gradations cannot be used for estimation of the X -induced (or any other type of) error trend: they are inevitably affected by various other factors that contribute to the wind measurement error. Hence in order to obtain a preliminary estimate of the strength of the trend, we had to subject the data to the traditional linear regression analysis. For the first trial, the data from all six groups were employed, and for the second trial, the (highly disperse) data of group 1 were excluded. The calculations yielded a stable linear trend about 0.5 m/s per 100 km of X , for both cases. Naturally, the correlation coefficient was very low (-0.18 and -0.26 , respectively), reflecting the large total variance of the SASS-NDBC wind speed difference (2 m/s).

3.4. Analysis of the Trend

The low quality of the input data does not permit quantitative analysis of the physical mechanisms causing the error trend. Furthermore, the number of cases contained in the interesting groups is insufficient to infer the influence of such important factors as the incidence angle and polarization of the transmitted/received signal. However, a preliminary hypothetical explanation can be put forth (sections 4 and 5) based on the following qualitative analysis of the trend.

We start by plotting the “true” wind U_b and the SASS wind U_s against the generalized wind fetch X . Since the confidence intervals for X remain the same as in Figure 2, we plot in Figure 3 only the mean values for each of the six groups. Let us notice that the SASS algorithms calculate the wind speed as a monotonically increasing function of the radar cross section: the common assumption is $\sigma^0 = AU^\alpha$ with A and α independent of U . Hence U_s can be viewed as a measure of the radar return, and according to our data, the latter turns out to be a function of two variables:

$$\sigma^0 = F(X, U_b) \quad (11)$$

The most conspicuous feature of the plot is the growth of U_s versus X , commencing at the inflection point $X \approx 130$ km.

This implied increase of σ^0 with a decreasing degree of wind-wave coupling is accompanied by either constant or decreasing actual wind U_b . Only when the wind is fairly high (the cases with $X < 130$ km) does σ^0 behave, at least qualitatively, in accord with the two-scale model of surface scattering: the radar return increases with the actual wind speed regardless of the change in the wind fetch. Since the postinflection portion that is based on 98% of all observations obscures the traditional view of the wind’s exclusive role in the scatterometer return, a question arises as to the mechanism that causes an impact of the wind-wave coupling measure X on the backscattering coefficient.

As Figure 3 shows, the quantity $\partial X/\partial U_b$ is never positive, while at the fetch-limited wave growth it is always negative in virtue of (8). Therefore the inflection point in Figure 3 signifies a competition between the two terms on the right-hand side of

$$d\sigma^0/dU_b = (\partial\sigma^0/\partial X)\partial X/\partial U_b + \partial\sigma^0/\partial U_b \quad (12)$$

The plot shows that the relative contribution of the X -related mechanism into the total backscatter becomes more important at large values of the generalized fetch.

4. GEOMETRICAL FEATURES OF SEA SURFACE IN RELATION TO THE FACTORS OF WIND WAVE DEVELOPMENT

In what follows, we imply cases where an equilibrium range in wave spectra has been established. For the extreme cases of large and small X , two limiting regimes of wind-wave coupling, weak and strong, are discussed in this section. These regimes are suggested to yield two different types of surface geometry. The general case of an intermediate fetch is considered by using the theory of incomplete self-similarity proposed by *Barenblatt and Leykin* [1981]. Finally, we deduce relevant implications for sea surface geometry by appealing to a concept of fractal (Hausdorff) dimension. This review will facilitate the interpretation of our experimental data, presented in section 5.

TABLE 4. Statistics of SASS Error Bias

Group	Number of Cases N	Centered Mean		Standard Deviation of e , m/s	Standard Deviation of X , km
		Error \bar{e} , m/s	Mean Generalized Fetch \bar{X} , km		
1	14	-5.2	244	1.2	155
2	54	-2.8	244	0.5	220
3	180	-0.8	205	0.5	193
4	217	0.8	172	0.5	175
5	73	2.6	149	0.5	139
6	12	4.8	81	1.0	42

TABLE 5. Statistics of SASS Error Bias After Deleting the Outliers

Group	Number of Cases N	Centered Mean Error \bar{e} , m/s	Mean Generalized Fetch \bar{X} , km	Standard Deviation of e , m/s	Standard Deviation of X , km
1	13	-5.2	219	1.2	132
2	52	-2.8	213	0.5	153
3	172	-0.8	175	0.5	129
4	205	0.8	138	0.5	90
5	70	2.6	128	0.5	91
6	12	4.8	81	1.0	42

4.1. Weak Versus Strong Wind-Wave Coupling Regimes

It is useful to have a criterion, however coarse, separating the two regimes. Consider the ratio C_0/U of the phase speed of the dominant wave to the mean wind velocity. When the wind-wave coupling is strong, the energy and momentum are transferred from the wind directly to the energy-carrying waves whose frequencies are close to that of the spectral peak, in the fashion of the Miles mechanism. Hence the phase speed of the spectral peak component is determined largely by the mean wind velocity: $\omega_0 \sim g/U$. In an equilibrium state, the weakly nonlinear, resonant wave-wave interactions are negligibly small compared to the source terms, i.e., to the energy input and dissipation due to wave breaking, and their main role is to slightly shift the spectral peak toward lower wave numbers as a result of a slow transfer of wave spectral energy from the "generation range" [Hasselmann, 1962]. This shift increases with the fetch: the weak effect of the wave-wave interactions accumulates with fetch very slowly, and its quantitative expression is given by (A4).

Assuming the linear-wave dispersion relation, one estimates C_0 as $\omega_0/k_0 = g/\omega_0$. Ultimately, (A4) and (A5) yield

$$\frac{C_0}{U} = (2.84 \times 2\pi)^{-1} \bar{x}^{0.3} \quad (13)$$

where x is nondimensional fetch. The strong wind-wave coupling corresponds to C_0 being much smaller than U , whereas the opposite case implies that the ratio (13) is greater than unity. Let us take $C_0/U = 1$ as a boundary between the two regimes. This yields the critical value of the nondimensional fetch to be 1.5×10^4 , and equation (A5) yields the critical

value of the generalized fetch X :

$$X_{cr} = x_{cr} U^2/g \approx 1.5 \times 10^4 U^2/g \quad (14)$$

Thus, for example, at winds under 10 m/s, the waves are strongly coupled with the wind if the fetch is well below 150 km.

4.2. The Weak Turbulence Theory of Equilibrium Wave Spectra

In the opposite limiting case of a well-developed sea (large fetch), the spectral density of the energy flux from wind to waves is greatest at frequencies well above the spectral peak. Zakharov and Zaslavskii [1982b] estimate the characteristic wave number for the "energy production range" as $k_\beta \approx 10g/U^2$, which is at least an order of magnitude greater than k_0 of the spectral peak. In their model, the wind input at lower frequencies is neglected altogether. The dissipation due to wave breaking becomes important at frequencies that are even higher than k_β . Finally, the rates of local and advective changes of the wave action spectral density are negligibly small because the time and spatial coordinates are scaled by wind duration and fetch, respectively. This leaves control of the equilibrium range almost exclusively to the wave-wave interactions. Because of these interactions, part of the energy supplied initially by turbulent wind at frequencies close to k_β is cascaded up the spectrum [Zakharov and Lvov, 1975; Zakharov and Zaslavskii, 1982a; Kitaigorodskii, 1983, 1987]. Because of the conservative nature of these weakly nonlinear interactions, the corresponding equilibrium range is called the Kolmogorov spectrum [Zakharov and Zaslavskii, 1982a]. However, unlike Kolmogorov's inertial subrange in isotropic

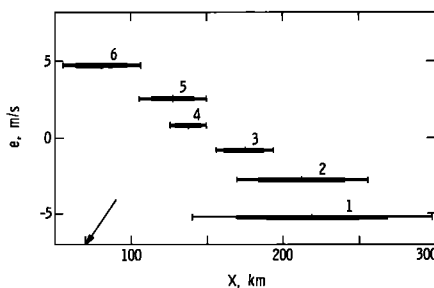


Fig. 2. The super observations of the NDBC-SASS wind speed difference against the generalized wind fetch (equation (8)), with confidence intervals for 80% (thick lines) and 95% (thin lines) significance levels. The group numbers displayed at each super observation correspond to the convention of Table 1. The tick mark indicated by the arrow shows the upper boundary of the wind fetch range covered by the experiment of Ross and Jones [1978].

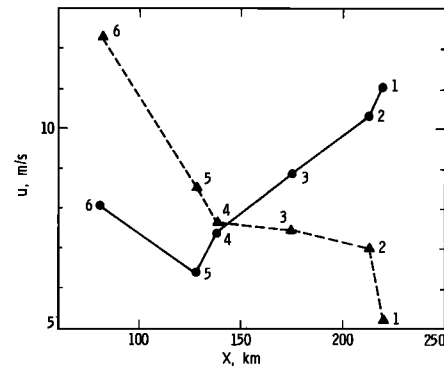


Fig. 3. The super observations of wind speed by NDBC (triangles) and SASS (circles), referred to 10-m height, against the generalized wind fetch X . The connecting lines are drawn to designate the trends. The group numbers displayed at each super observation correspond to the convention of Table 1.

turbulence, the energy cascade is inverse and, in this sense, is similar to the case of two-dimensional turbulence. The requirement of conservation of the wave action flux density, which is roughly satisfied for the weak nonlinear interactions, results in the Zakharov equilibrium law for this inertial subrange [Zakharov and L'vov, 1975; Zakharov and Zaslavskii, 1982a; Kitaigorodskii, 1983]:

$$F(k) \sim \beta p^{1/3} k^{-10/3} \tag{15}$$

where β is a proportionality coefficient, evaluated by Zakharov and Zaslavskii [1983] as $\beta \approx 0.83$, and p is the wave action flux (which is conserved).

The dominance of the resonant wave-wave interactions occurring within wave tetrads results in an appreciable coupling among the corresponding Fourier harmonics. As a result, the odd-order statistical moments appear. The third-order correlations and bispectra can be readily evaluated (see, for example, Hasselmann et al., [1963] and Holloway, 1986). The resulting weakly non-Gaussian field of sea surface elevation is characterized by a broad spectrum and marked asymmetry of the wave profile about the zero-valued horizontal plane (Figure 4).

4.3. Possible Generalizations and the Wave Action Flux

Other power laws have also been proposed on various grounds [e.g., Zakharov and Filonenko, 1966; Toba, 1973; Donelan et al., 1985; Phillips, 1985], and several attempts are known at introducing a general "universal" form of wave spectrum in which the power law exponent is determined by external conditions [Barenblatt and Leykin, 1981; Huang et al., 1981; Liu, 1983]. The Barenblatt-Leykin spectrum is based on Barenblatt's [1979] theory of incomplete self-similarity. The universal form for the equilibrium range is controlled by the degree of wind-wave development:

$$S(\omega) = g^{-2-\mu} \omega^{-(5-\mu)} U^\mu \Phi(gX/U^2) \tag{16a}$$

The corresponding wave number spectrum for deep water waves readily follows from (16a) and dimensional considerations:

$$F(k) = g^{-\mu/2} U^\mu k^{-(8-\mu)/2} \Phi_1(gX/U^2) \tag{16b}$$

As suggested by Barenblatt and Leykin, μ is a universal function of the nondimensional fetch x :

$$\mu = \mu(gX/U^2) = \mu(x) \tag{17}$$

and so are Φ and Φ_1 .

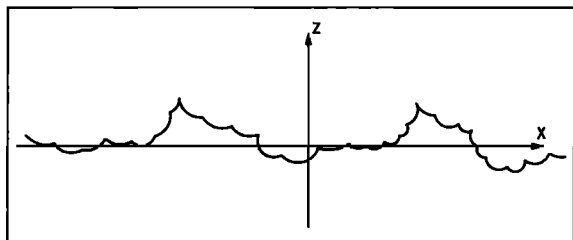


Fig. 4. Sketch of a wave profile characterized by large surface density of statistically similar wavelets: a cascade pattern in surface topography (for more detail see Glazman [1986]).

In these equations we took the liberty of replacing the Barenblatt and Leykin parameter of length Λ (which they associate with the "length of the energy-bearing low-frequency waves") with the parameter X that we refer to as the generalized wind fetch. Equations (16) yield the traditional Phillips spectrum at $\mu = 0$, and the Zakharov-Zaslavskii spectrum is obtained at $\mu = 4/3$. These two values can be viewed as the extreme cases of very strong and very weak wind-wave coupling, respectively:

$$\lim_{x \rightarrow 0} \mu(x) = 0 \quad \lim_{x \rightarrow \infty} \mu(x) = 4/3 \tag{18}$$

In the latter case, comparison of (15) and (16b) yields

$$\lim_{x \rightarrow \infty} p(x) = \beta^{-1} \Phi(\infty) g^{-2} U^4 \tag{19}$$

In the absence of large-fetch data, neither Barenblatt and Leykin nor Huang et al. [1981] have been able to correctly relate the exponent μ and the "Phillips constant" Φ to external conditions. At present, such experimental data are becoming available: Figure 5 shows the results reported by Donelan et al. [1985] confirming the tendency of μ to increase with x .

4.4. Fractal Dimension and Wavelet Statistics

Kitaigorodskii [1987] pointed out that the basic power laws describing the equilibrium range of wave spectra for the short-fetch and long-fetch situations are not much different. More precisely, the envelope containing the corresponding curves is very narrow. However, as is claimed in this section, even insignificant variations of the exponent in the power law (equation (16b)) have great implications for a surface's geometrical properties.

Here, we are interested mainly in the rate of steep wavelet occurrence. The formal approach to the problem of wavelet statistics has been presented earlier [Glazman, 1986], and a mathematical treatment on surface features associated with the equilibrium range of wave spectra has been delineated by Glazman [1988]. Let us now focus on a qualitative aspect of the problem and highlight the fact that the Phillips law (k^{-4}), viewed in our model as the limiting case corresponding to the strong wind-wave coupling, marks the boundary separating two essentially different regimes of surface geometry, fractal and nonfractal. For applications and theory of the Hausdorff dimension D_H , the reader is referred to Mandelbrot [1983] and Adler [1981].

Considering only the large-scale (in the sense of section 2) features of a normal random surface, this dimension is found as [Glazman, 1988]

$$D_H = \frac{8 - Q}{2} \tag{20}$$

where Q is the exponent in the power law for the wave number spectrum. In the notation of (16b), $Q = [8 - \mu(x)]/2$, which yields

$$D_H = 2 + \frac{\mu(x)}{4} \tag{21}$$

This provides a simple interpretation of $\mu(x)$: $\mu/4$ represents a fractal codimension of the sea surface. Hence the Phillips law corresponds to $D_H = 2$ which is referred to as a marginal fractal (Berry's [1979] terminology), and the Zakharov law (equa-

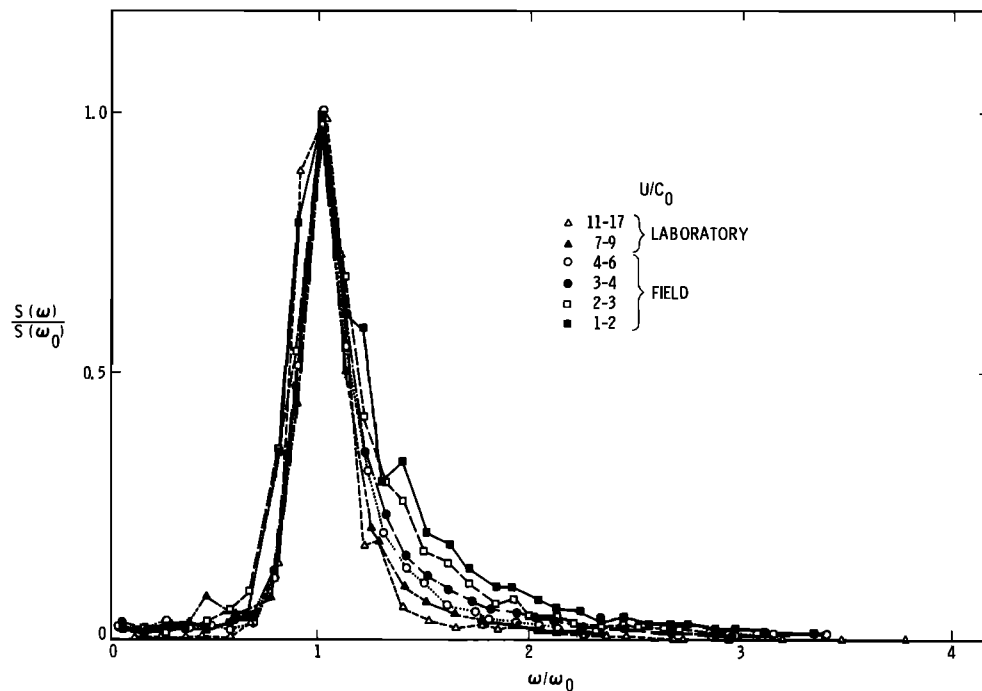


Fig. 5. Normalized frequency spectra grouped into classes by U/C_0 . (Reproduced from *Donelan et al.* [1985], courtesy of *Philosophical Transactions of the Royal Society of London*).

tion (15)) yields $D_H = 2.333$, which represents an essentially fractal regime. In general, the fractal dimension is a monotonically increasing function of the degree of sea maturity.

A fractal surface can be constructed by a cascade process (Figure 4), whereby a narrow-banded random surface ζ_1 with the characteristic wavelength λ_1 is superimposed on the original, narrow-banded, surface ζ_0 (thereafter called the "basic wave"), whose characteristic wavelength $\lambda_0 > \lambda_1$. (A surface is considered to be narrow-banded if its wave number spectrum decays faster than k^{-4} ; such a surface is differentiable.) Here, λ_0 represents the low-frequency cutoff of the resultant fractal surface. This cascade process is repeated an infinite number of times using smaller and smaller λ_i . Practically, the construction is terminated at a sufficiently small λ_N ($\lambda_N \ll \lambda_0$) called the microscale. There are certain requirements, e.g., statistical similarity of the constituent surfaces, a continuous range of λ_i values and a limit on the rate of decrease for the characteristic amplitude of the constituent surfaces, that must be satisfied. Although the cascade process stops on achieving the microscale, it is intuitively clear that it results in a dramatic increase in the mean number of wave crests per unit area (and per basic wave) as compared with a regular, nonfractal, surface.

In fact, it can be deduced analytically or calculated based on simulations of a surface's realizations [Glazman, 1986, 1988] that starting from $D_H = 2$, the mean number of wave crests per basic wave becomes a rapidly increasing function of the fractal dimension. Hence we anticipate an explosive growth in the surface density of wavelet occurrence as soon as $\mu(x)$ departs from zero as the wind-wave coupling decreases.

When the assumption of a surface's normality is dropped, the techniques of evaluating the fractal dimension and wavelet statistics, mentioned above, are not applicable. Hence the results pertaining to Gaussian surfaces may be employed only as a first approximation.

5. EXPLANATION OF THE X-RELATED BIAS

Our hypothetical explanation is based on the view proposed in the preceding section that the fractal dimension and, thereby, the surface density of steep wavelet occurrence increase rapidly as wind waves develop. We assume the total cross section of the radar backscatter to consist of the two contributions, the Bragg component and the spike component:

$$\sigma^0 = \sigma_B^0 + \sigma_s^0 \quad (22)$$

The former represents the diffuse scatter by the Bragg-type resonant small-scale ripples riding on the large-scale waves while the latter, described tentatively by (2), is associated with individual sufficiently steep large-scale wavelets.

5.1. Interpretation of Figure 3

The relative importance of the second component increases with the degree of wave development. When X given by (7) is small (the wind-wave coupling is strong), the mean number of ringing wavelets per unit surface area is too low to produce an effect comparable to the background diffuse scattering. Consequently, the registered backscatter will behave as if it were due entirely to the diffuse scattering. The preinflection portion of the experimental curve in Figure 3 reflects this behavior. However, at greater values of X the second term in (22) yields an appreciable contribution to the total backscatter. In contrast to σ_B^0 which, being caused by the small-scale ripples, is controlled primarily by the local wind speed, the spike component is a function of both the local and the nonlocal factors of wind wave development. This is due to the fact that the probability (4) for a given wavelet to be sufficiently steep is a (exponentially) strong function of the rms slope of the large-scale waves. Hence although the rms slope itself may depend only weakly on the wave maturity (as was discussed in section 2.1

in connection with the two-scale model of surface scattering), the rate of steep wavelet occurrence (equation (3)) is a strong function of the long-range wind wave factors. Particularly, one may write:

$$\sigma_s^0 = F(X, U) \quad (23)$$

This equation could be verified experimentally by selecting the cases which differ mainly in the values of X . Points 2 through 5 in Figure 3 are characterized by very small variations in the mean wind speed and by sufficiently large values of X that must correspond to $D_H > 2$. Hence this postinflection segment of the experimental curve can be taken as an illustration of our assertion. (Point 1, which is based on low-wind cases, represents too small and too scattered a cluster of observations and, for the sake of simplicity, is excluded from the present discussion.)

5.2. The Mechanism of Radar Spikes

Neither the experimental data nor the theoretical considerations employed so far shed light on the nature of σ^1 in (2). However, two candidate mechanisms of spike generation, which are frequently considered in the remote sensing literature, might well fit the hypothetical qualitative model (equation (2)) discussed in section 2.1. The first one is the mechanism of wedge scattering whereby the backscatter is caused by the diffraction of the em wave at the wedgelike crest of a water wavelet [e.g., Lyzenga et al., 1983; Kwoh and Lake, 1984]. The second is the mechanism of "gentle breaking" of sufficiently steep wavelets which results in a locally increased small-scale surface roughness appearing near the breaking wave crest, which yields an intense diffuse scatter [Banner and Fooks, 1985] from the breaking region. The wave breaking also results in a relatively high surface density of specularly oriented (centimeter size) facets [Kwoh and Lake, 1984, 1985] emerging at the breaking crest.

The inception of breaking is controlled largely by the steepness of a wavelet, hence by external factors of wind wave evolution. However, once the wavelet has attained the breaking conditions, the impact of external factors on the ensuing development of the small-scale surface features is insignificant. This prompts the suggestion that the only parameter that influences the development of the breaking region is Γ . However, its value must be close to the breaking wave criterion:

$$\sigma^1 = f(\Gamma) \approx f(\Gamma_{cr}) + (\partial f / \partial \Gamma)(\Gamma - \Gamma_{cr}) \quad (24)$$

Hence in the first approximation, σ^1 can be taken outside the internal integral in (2), and the problem of relating the spike component to the external conditions thus reduces to the evaluation of steep wavelet statistics.

In the case of the wedge-diffraction mechanism, a similar argument applies: a wave has to attain a critical steepness to have a sufficiently sharp crest causing diffraction. Since the critical steepness of gravity waves is constrained (say, as in the Stokes wave), the variability of the resulting σ^1 is very limited.

Other possible mechanisms of sea spikes, for instance whitecaps, might present a more complicated problem: the lifetime and size of a whitecap appreciably depend on the dimensions of a breaking wave [Duncan, 1981]. However, instead of speculating about the implications of these factors for the range of σ^1 variations, we refer the reader to a recent dis-

ussion on this and related topics by Donelan and Pierson [1987].

6. SUMMARY AND CONCLUSIONS

Based on a set of SASS-NDBC colocated observations, a trend in the SASS wind speed error is found as related to the degree of development of wind-generated gravity waves. This trend, whose preliminary estimate is given as 0.5 m/s per 100 km of the generalized wind fetch, is capable of introducing a well-pronounced environmental bias into the scatterometer-produced global distributions of wind. The low quality and insufficient number of the SASS and NDBC colocated observations did not allow us to conduct a detailed study of the specific physical mechanisms responsible for the trend. Instead, a qualitative analysis of the data is presented based on super observations obtained by ordering the available data by gradations of error. This analysis is supported by theoretical considerations on pertinent aspects of wind-wave dynamics and sea surface statistical geometry.

We adopt a view that in a sufficiently developed sea, the surface topography assumes a cascade pattern resulting in an increased number of wave crests (wavelets) per basic wave. This leads to an increased probability of occurrence of steep wavelets capable of producing a spike in the radar return. Based on a simplified (Gaussian) theoretical model and, also, appealing to the concept of fractal dimension of a rough surface, the surface density of such "ringing" wavelet events is suggested to be a rapidly increasing function of the degree of wind wave development. Our conclusion agrees with a hypothesis which is now becoming commonly accepted that a backscattered X band, and very possibly C band, signal includes two major components. One is due to Bragg-type diffuse scattering caused by the small-scale ripples. The other is due to intermittently occurring spikes in the radar backscatter. We think that while the first component is controlled primarily by the local instantaneous wind, the second is strongly affected (in the first approximation, exponentially dependent on the reciprocal of the wave slope variance) by the degree of wind wave development. This component, which becomes particularly important in a sufficiently developed sea, is deemed responsible for the influence of nonlocal factors, such as wind fetch, on the scatterometer measurements.

We agree with Woiceshyn et al. [1986] that the model functions presently available do not uniformly meet the instrument performance requirements.

The trend found in the present work does not exclude the possibility of other biases in scatterometer winds, as for example a SST-caused bias occurring at low wind speeds. However, unlike other biases, the X -induced trend appears to be a widespread phenomenon manifested at all wind speeds, all values of the generalized wind fetch, and many geographical locations covered by the NDBC data employed in this work.

The largely qualitative model set forth in sections 2, 4, and 5 should be substantiated by studying the roles of polarization and incidence angle in the discovered error trend. However, owing to the insufficient number and low quality of the available observations this task had to be postponed. Since the physical factors deemed to be responsible for the error trend are connected with certain fundamental properties of the wave field under open ocean conditions, their further study appears to be of great potential benefit with regard to satellite scat-

terometry as well as in connection with many other microwave remote sensing techniques.

APPENDIX

Since the X defined by (7) has the dimension of length and the meaning similar to the traditional wind fetch, it is reasonable to try selecting the proportionality coefficient const so as to match this X to the conventional fetch \bar{X} . Evidently, the success is guaranteed only in the special case of a steady, spatially uniform wind blowing off the coast and only if the actual potential energy density of waves is a linear function of the conventional wind fetch. The latter condition can be satisfied if the fetch is not too large. Indeed, it turns out that a parameterization offered by Hasselmann *et al.* [1976] for the "mean" JONSWAP spectrum satisfies the condition of additivity of the wave energy density with respect to the wind fetch.

Using the mean JONSWAP spectrum with its two most changeable variables, the Phillips constant α and the spectrum peak frequency ω_0 expressed through wind fetch and wind speed, one can relate the significant wave height $H_{1/3}$ to the environmental conditions:

$$\frac{H_{1/3}^2}{16} \approx \langle \zeta^2 \rangle = \int_0^\infty S(\omega) d\omega \quad (\text{A1})$$

Introducing the nondimensional frequency, $\Omega = \omega/\omega_0$, the last equality can be written as

$$\langle \zeta^2 \rangle = \alpha g^2 \omega_0^{-4} m_0 \quad (\text{A2})$$

where $m_0 = \int_0^\infty s(\Omega) d\Omega$ and $s(\Omega)$ is a nondimensionalized JONSWAP spectrum. The value of m_0 has been calculated to be 0.2816 by Glazman [1986]. The Phillips constant and the spectral peak frequency are related to the conventional wind fetch \bar{X} and wind speed U [Hasselmann *et al.*, 1976] by

$$\alpha = 0.0662 \bar{x}^{-0.2} \quad (\text{A3})$$

$$\omega_0 = 2.84 \cdot 2\pi \frac{g}{U} \bar{x}^{-0.3} \quad (\text{A4})$$

where

$$\bar{x} = g\bar{X}/U^2 \quad (\text{A5})$$

Equations (A1) through (A5) yield

$$H_{1/3} = 1.715 \times 10^{-3} \frac{U^2 \bar{x}^{1/2}}{g} = 1.715 \times 10^{-3} \frac{\bar{X}^{1/2} U}{g^{1/2}} \quad (\text{A6})$$

Identifying \bar{X} with the X of (7) yields equation (8) of section 2 and const = 26.1.

Contrary to what one might expect, the proportionality coefficients in (A6) (hence the value of X in (8)) does not change dramatically when the other three parameters of the JONSWAP spectrum change. Let us, for instance, take m_0 as corresponds to the limiting case of the JONSWAP spectrum attained in a "fully developed sea." According to the original notion, this limiting form is given by the Pierson-Moskovitz spectrum. Then the calculations [Glazman, 1986] yield $m_0 = 0.1848$. This results in const ≈ 40 , rather than in an infinitely (or just very) large number necessary to produce an infinite (or just very large) fetch.

Thus (8) should be viewed only as a crude estimate of the fetch which is accurate at small values of X . As the actual

fetch increases, the wave potential energy will cease to be an linear function of the fetch \bar{X} , and the geometrical interpretation of X in (7) as the conventional wind fetch will become inappropriate.

Acknowledgments. This work was performed at the Jet Propulsion Laboratory, California Institute of Technology, under contract with the National Aeronautic and Space Administration.

REFERENCES

- Adler, R. J., *The Geometry of Random Fields*, 279 pp., John Wiley, New York, 1981.
- Banner, M. L., and E. H. Fooks, On the microwave reflectivity of small-scale breaking water waves, *Proc. R. Soc. London, Ser. A*, 399, 93–109, 1985.
- Barenblatt, G. I., *Similarity, Self-Similarity, and Intermediate Asymptotics*, 218 pp., Consultant Bureau, New York, 1979.
- Barenblatt, G. I., and I. A. Leykin, On the self-similar spectra of wind waves in the high-frequency range, *Izv. Acad. Sci. USSR Atmos. Oceanic Phys., Eng. Transl.*, 17(1), 35–41, 1981.
- Berry, M. V., Diffraction, *J. Phys. A*, 12(6), 781–796, 1979.
- Brown, R. A., On satellite scatterometer capabilities in air-sea interaction, *J. Geophys. Res.*, 91(C2), 2221–2232, 1986.
- Donelan, M. A., and W. J. Pierson, Radar scattering and equilibrium ranges in wind-generated waves with application to scatterometry, *J. Geophys. Res.*, 92(C5), 4971–5029, 1987.
- Donelan, M. A., J. Hamilton, and W. H. Hui, Directional spectra of wind generated waves, *Philos. Trans. R. Soc. London, Ser. A*, 315, 509–562, 1985.
- Duncan, J. H., An experimental investigation of breaking waves produced by a towed hydrofoil, *Proc. R. Soc. London, Ser. A*, 377, 331–348, 1981.
- Freilich, M. H., Satellite scatterometer comparisons with surface measurements: techniques and SEASAT results, Proceedings of the ERS-1 Wind and Wave Calibration Workshop, *Eur. Space Agency Spec. Publ.*, SP-262, 57–62, 1986.
- Glazman, R. E., Statistical characterization of sea surface geometry for a wave slope field discontinuous in the mean square, *J. Geophys. Res.*, 91(C5), 6629–6641, 1986.
- Glazman, R. E. Fractal nature of surface geometry in a developed sea, in *Proceedings of the Workshop on Scaling, Fractals and Non-Linear Variability in Geophysics*, edited by S. Lovejoy and D. Schertzer, D. Reidel, Hingham, Mass., in press, 1988.
- Hasselmann, K., On the non-linear energy transfer in a gravity wave spectrum, 1, *J. Fluid Mech.*, 12, 481–500, 1962.
- Hasselmann, K., W. Munk, and G. MacDonald, Bispectra of ocean waves, in *Proceedings of the Symposium on Time Series Analysis*, edited by M. Rosenblatt, pp. 125–140, John Wiley, New York, 1963.
- Hasselmann, K., D. B. Ross, P. Muller, and W. Sell, A parametric wave prediction model, *J. Phys. Oceanogr.*, 6, 200–228, 1976.
- Holloway, G., Eddies, waves, circulation and mixing: Statistical geofluid mechanics, *Annu. Rev. Fluid Mech.*, 18, 60–91, 1986.
- Huang, N. E., S. R. Long, C.-C. Tung, Y. Yuen, and L. F. Bliven, A unified two-parameter wave spectral model for a general sea state, *J. Fluid Mech.*, 112, 203–224, 1981.
- Jones, W. L., L. C. Schroeder, D. H. Boggs, E. M. Bracalente, R. A. Brown, G. J. Dome, W. J. Pierson, and F. J. Wentz, The Seasat-A satellite scatterometer: The geophysical evaluation of remotely sensed wind vectors over the ocean, *J. Geophys. Res.*, 87(C5), 3297–3317, 1982.
- Kalmykov, A. I., and V. V. Pustovoytenko, On polarization features of radio signals scattered from the sea surface at small grazing angles, *J. Geophys. Res.*, 81, 1960–1964, 1976.
- Keller, W. C., W. J. Plant, and D. Weissman, The dependence of X band microwave sea return on atmospheric stability and sea state, *J. Geophys. Res.*, 90(C1), 1019–1029, 1985.
- Kitaigorodskii, S. A., On the theory of the equilibrium range in the spectrum of wind-generated gravity waves, *J. Phys. Oceanogr.*, 13, 816–827, 1983.
- Kitaigorodskii, S. A., A general explanation of the quasi-universal

- form of the spectra of wind-generated gravity waves at different stages of their development *APL Tech. Dig.*, 8(1) 11–15, 1987.
- Kwoh, D. S., and B. M. Lake, A deterministic, coherent and dual-polarized laboratory study of microwave backscattering from water waves, 1, Short gravity waves without wind, *IEEE J. Oceanic Eng.*, OE-9, 291–308, 1984.
- Kwoh, D. S., and B. M. Lake, The nature of microwave backscattering from water waves, in *The Ocean Surface: Wave Breaking, Turbulent Mixing and Radio Probing*, edited by Y. Toba and H. Mitsuyasu, pp. 249–256, D. Reidel, Hingham, Mass., 1985.
- Liu, P. C., A representation for the frequency spectrum of wind-generated waves, *Ocean Eng.*, 6, 429–441, 1983.
- Liu, W. T., The effects of the variations in sea surface temperature and atmospheric stability in the estimation of average wind speed by SEASAT-SASS, *J. Phys. Oceanogr.*, 14(2), 392–401, 1984.
- Liu, W. T., K. B. Katsaros, and J. B. Businger, Bulk parameterizations of air-sea exchanges of heat and water vapor including the molecular constraints at the interface, *J. Atmos. Sci.*, 36, 1722–1735, 1979.
- Lyzenga, D. R., A. L. Maffett, and R. A. Schuchman, The contribution of wedge scattering to the radar cross section of the ocean surface, *IEEE Trans. Geosci. Remote Sens.*, GE-21(4), 502–505, 1983.
- Mandelbrot, B. B., *The Fractal Geometry of Nature*, 468 pp., W. H. Freeman, San Francisco, Calif., 1983.
- Phillips, O. M., On the dynamics of unsteady gravity waves of finite amplitude, *J. Fluid Mech.*, 9, 193–217, 1960.
- Phillips, O. M., Spectral and statistical properties of the equilibrium range in wind-generated gravity waves, *J. Fluid Mech.*, 156, 505–531, 1985.
- Plant, W. J., W. C. Keller, and A. Cross, Parametric dependence of ocean wave-radar modulation transfer functions, *J. Geophys. Res.*, 88, 9747–9756, 1983.
- Ross, D., and W. L. Jones, On the relationship of radar backscatter to wind speed and fetch, *Boundary Layer Meteorol.*, 13, 151–163, 1978.
- Skolnik, M., *Introduction to Radar Systems*, 581 pp., McGraw-Hill, New York, 1980.
- Toba, Y., Local balance in the air-sea boundary processes, III, On the spectrum of wind waves, *J. Oceanogr. Soc. Jpn.*, 29, 209–220, 1973.
- Woiceshyn, P. M., M. G. Wurtele, D. H. Boggs, L. F. McGoldric, and S. Peteherych, The necessity for a new parameterization of an empirical model for wind/ocean scatterometry, *J. Geophys. Res.*, 91(C2), 2273–2288, 1986.
- Wright, J. W., A new model for sea clutter, *IEEE Trans. Antennas Propag.*, AP-16, 217–223, 1968.
- Zakharov, V. E., and N. N. Filonenko, The energy spectrum for stochastic oscillation of a fluid's surface (in Russian), *Dokl. Acad. Nauk SSSR*, 170(6), 1292–1295, 1966.
- Zakharov, V. E., and V. S. L'vov, Statistical description of non-linear wave fields, *Radiophys. Quantum Electron.*, Engl. Transl., 18, 1084–1097, 1975.
- Zakharov, V. E., and M. M. Zaslavskii, The kinetic equation and Kolmogorov spectra in the weak turbulence theory of wind waves, *Izv. Acad. Sci. USSR Atmos. Oceanic Phys.*, English Transl., 18(9), 747–753, 1982a.
- Zakharov, V. E., and M. M. Zaslavskii, Ranges for generation and dissipation in the kinetic equation for a low-turbulence theory of wind waves, *Izv. Acad. Sci. USSR Atmos. Oceanic Phys.*, English Transl., 18(10), 821–827, 1982b.
- Zakharov, V. E., and M. M. Zaslavskii, Shape of the spectrum of energy carrying components of a water surface in the weak-turbulence theory of wind waves, *Izv. Acad. Sci. USSR Atmos. Oceanic Phys.*, English Transl., 19(3), 207–212, 1983.

R. E. Glazman, Jet Propulsion Laboratory, California Institute of Technology, 4800 Oak Grove Drive, Pasadena, CA 91109.

J. Ip, Dartmouth College, Hanover, NH 03755.

G. G. Pihos, Aerospace Corporation, P.O. Box 92957, Los Angeles, CA 90009.

(Received December 10, 1986;
accepted October 7, 1987.)